Evolution of Microstructure and Texture during Casting of AISI 304 Stainless Steel Strip

A. HUNTER and M. FERRY

The solidification behavior of AISI 304 stainless steel strip was studied using a melt/substrate contact apparatus, whereby a copper substrate embedded in a moving paddle is rapidly immersed into a steel melt to produce thin (~1-mm gage) as-cast coupons. For cases where other casting conditions were kept constant, the effect of substrate topography and melt superheat on the development of microstructure and texture during solidification was studied using electron backscatter diffraction (EBSD) and optical microscopy. It was found that nucleation and growth of grains during solidification were influenced both by substrate topography and melt superheat. A ridged substrate produced a high density of randomly oriented grains at the chill surface with the preferred growth of ⟨001⟩-oriented grains perpendicular to the substrate wall producing a coarse columnar grain structure exhibiting a strong ⟨001⟩ fiber texture at the strip center. In contrast, a smooth substrate resulted in a lower nucleation density to produce a very coarse-grained columnar microstructure with moderate and essentially constant ⟨001⟩ fiber texture throughout the strip thickness. By the manipulation of casting parameters, it is possible to produce strip-cast austenitic stainless steel with a particular microstructure and texture.

I. INTRODUCTION

DIRECT strip casting (DSC) to produce as-cast steel sheet has attracted much attention because this technology has the capability of producing lower cost products compared with conventional continuous casting (CCC) and thermomechanical processing (TMP) routes.[1] Twin roll casting (TRC) is becoming the favored method of casting steel strip.[2] In this process, molten metal is introduced into a tundish, which flows through a nozzle into the gap between two water-cooled copper rolls that rotate at a given speed to produce strip of thickness of 1 to 2 mm. The high rate of heat extraction from the melt through the rolls results in rapid solidification and produces as-cast steel microstructures radically different to those produced by CCC/TMP.[2–5] In light of these differences, it is necessary to develop a better understanding of the influence of casting and other metallurgical variables associated with TRC on microstructural development of commercially significant steel grades.

An understanding of the nucleation and growth of phases during TRC of metals such as austenitic stainless steel (γ-SS) is important because it is anticipated that these steels will be produced in large tonnages by this route.[2] A notable example is AISI 304, which contains the principal alloying elements (mass pct) ~18Cr and ~8Ni, which infers, from the ternary phase diagram, [6] that the preferred nucleation phase is delta-ferrite (δ). However, splat quenching experiments have shown that austenite (γ) is the dominant nucleation and solidifying phase due to the high initial heat-transfer rate, which favors its formation.[7,8,9] The solidification behavior of this alloy during DSC is also expected to be complex,[2] so it is important to understand the effect of various casting conditions on microstructural development. In the present work, AISI 304 coupons were produced using a dip casting apparatus developed by Strezov,[10] which stimulates closely the conditions of TRC.[10,11] The aim is to investigate the nucleation and growth behavior of grains during solidification as an understanding of variables affecting the as-cast microstructure, and the texture of this steel grade is highly significant, because its commercial production by TRC is now being developed.[2]

A. HUNTER, Postgraduate Student, is with the Institute for Steel Processing and Products, University of Wollongong, Wollongong NSW 2522, Australia. M. FERRY, Senior Lecturer, is with the School of Materials Science and Engineering, University of New South Wales, Sydney NSW 2052, Australia. Contact e-mail: m.ferry@unsw.edu.au

Manuscript submitted February 19, 2002.

II. EXPERIMENTAL PROCEDURE

A. *Production of As-Cast Coupons*

An AISI 304 stainless steel with melt composition (mass pct) 17.65Cr, 8.35Ni, 0.039C, 1.0Mn, 0.36Si, 0.16Cu, 0.009Nb, 0.01S, and 0.003Ti was used in this work. The mechanisms of nucleation and growth of solidifying grains were studied using Strezov's melt/substrate contacting apparatus.[10] The technique produces as-cast steel coupons with a microstructure similar to that produced by TRC,[4,5,10,11] but has the advantage of systematically controlling important variables such as alloy composition, melt superheat, furnace atmosphere, casting speed, substrate type, and substrate topography.[11]

The melt/substrate contacting apparatus is shown schematically in Figure 1, indicating the immersion or "casting" direction (CD), transverse direction (TD), and normal direction (ND). Experiments were carried out using copper substrates embedded in a moveable paddle, which allows simultaneous immersion of substrates with different surface topographies. The substrate blocks were made from electrolytic tough pitch copper, and the surface was either prepared with 1200 grade SiC paper and surface treated to form an amorphous chromium layer, which produced a *smooth* surface finish of ~0.5 μm R_a or machined and Cr-coated to produce a *ridged* surface. In this technique, the paddle is accelerated through the melt surface to the required "casting

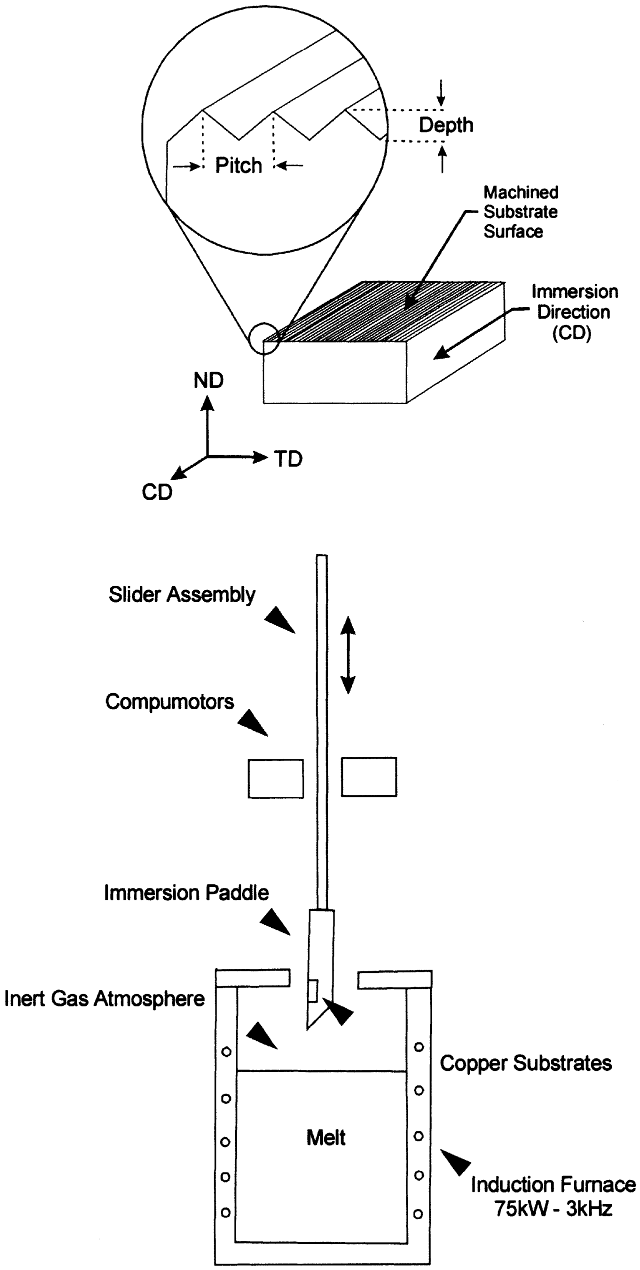

Fig. 1—Schematic diagrams of experimental apparatus for producing cast stainless steel coupons and substrate surface showing machined ridges parallel to the immersion (casting) direction. The casting and transverse directions are given as CD and TD, respectively, and the direction normal to the substrate surface is ND (figures reproduced from Ref. 11).

velocity" and travels at constant speed during the time that the substrate is in contact with the melt. The paddle is then retracted from the melt, to its home position above the furnace, where a solidified sheet sample is produced. This sample represents the solidification of one of the two shells that form during TRC.

To study the effect of substrate topography on nucleation and growth of grains during solidification, the depth and pitch of these ridges were varied (Table I and inset in Figure 1). In all cases, the casting direction was parallel to the ridges (Figure 1). Casting experiments were then carried out in an argon atmosphere using an immersion velocity of 0.5 m/s at a constant melt superheat of 10 °C, 50 °C, 90 °C, and 100 °C.

Table I. Casting Parameters and Average Thickness of As-Cast Coupons

Melt Superheat (°C)	Substrate Type (Depth × Pitch) (μm)	Sample Thickness (mm)
10	smooth	1.0
	20 × 180	0.8
	50 × 100	0.8
50	smooth	1.4
	20 × 180	1.0
	50 × 100	1.0
90	smooth	1.4
	20 × 180	1.0
	50 × 100	1.0
100	smooth	1.4
	20 × 180	1.0
	50 × 100	1.0

B. *Temperature and Heat-Transfer Measurements*

The measurement of both temperature and heat transfer during dip casting of γ-SS has been documented in detail by Strezov and Herbertson.[11] To monitor temperature during immersion, two 0.25-mm-diameter, type K, thermocouples were placed at a depth of 500 to 600 μm below the surface of each substrate block. The high response rates and acquisition times of the thermocouples allowed an acquisition rate of 2 kHz, which was sufficient to determine the temperature changes during the first 50 ms of melt/substrate contact, which corresponded to the initial stages of solidification. The transient interface heat flux pattern over this period of melt/substrate contact was calculated by Strezov[10] using a modified version of Beck's inverse heat conduction algorithm.[12]

C. *Characterization of Microstructure and Texture*

The development of microstructure and texture during solidification was investigated using optical microscopy and scanning electron microscopy (SEM). The ND-TD sections of as-cast coupons (Figure 1) were examined at a distance of 25 mm below the top edge of each as-cast coupon, which represents, for a paddle speed of 0.5 m/s, a residence time in the melt of 380 ms. Samples were mechanically ground, electrolytically polished, and etched in 10 pct oxalic acid to reveal nucleation sites, microsegregation, and grain structure. The strip or "chill" surface was prepared for microstructural examination by cleaning in a 10 pct HCl aqueous solution ultrasonically vibrated for 300 seconds to remove any surface oxide.

The solidification microstructure and texture were determined using a HKL electron backscatter diffraction (EBSD) facility interfaced to a scanning electron microscope. A quantitative description of texture development was gained, for a given casting condition, by EBSD analysis of individual grain orientations at various distances below the strip surface. The angular deviation (α) of a given crystallographic direction (i.e., $\langle 001 \rangle$) per grain can be determined as a function of some significant direction within the sample (i.e.,

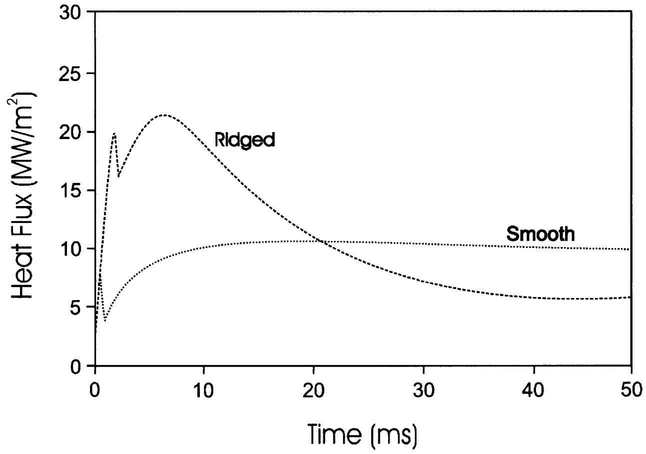

Fig. 2—Heat flux histories for samples solidified onto both a smooth and 30 × 180 μm ridged substrate at 50 °C melt superheat.[11]

ND). For cubic materials, the smallest angle α ($0 \leq \alpha \leq \pi/4$) that any given ⟨001⟩ direction makes with ND is given as $(\Phi^2 + \varphi_2^2)^{1/2}$ where Φ and φ_2 are Euler angles. For any number of grains (n), the mean angular deviation of primary ⟨001⟩ dendrite arm away from ND is given by

$$\overline{\alpha} = \frac{\sum_{i=1}^{n} (\Phi^2 + \varphi_2^2)_i^{1/2}}{n} \qquad [1]$$

Full details of the calculation method to generate $\overline{\alpha}$ for any given set of Euler angles is given elsewhere.[13] It will be shown in Section III that ridge dimensions (Table I) have only a small influence on microstructure and texture development. Therefore, more detailed studies of microstructural development of the as-cast strips were carried out on the smooth and 20 × 180 μm ridged substrates.

III. RESULTS

A. *Heat Transfer during the Initial Stages of Solidification*

Figure 2 gives typical heat-transfer results,[11] showing calculated heat flux histories for the initial 50 ms of contact with a smooth substrate and a typical ridged substrate (30-μm depth and 150-μm pitch). It is pertinent to note that Strezov[10] demonstrated that the variability in calculating the maximum heat flux and the overall shape of the heat flux curves after the peak to be ±0.25 and ±2 MW/m^2, respectively. Regardless of substrate topography, the maximum heat flux values were reached in about the first 10 ms of contact, and this was attributed to nucleation at the melt/substrate interface.[11] For constant casting speed, furnace atmosphere, and melt superheat, the maximum heat flux during solidification from a ridged substrate was 5 to 10 MW/m^2 greater than from a smooth substrate. Although these maximum heat fluxes were higher for the ridged substrate, the total heat transferred over the full immersion time (~380 ms) was higher for the smooth substrate. This resulted in a slightly thicker sample (Table I), which indicates that a smooth substrate generates a slightly higher *average* rate of solidification.

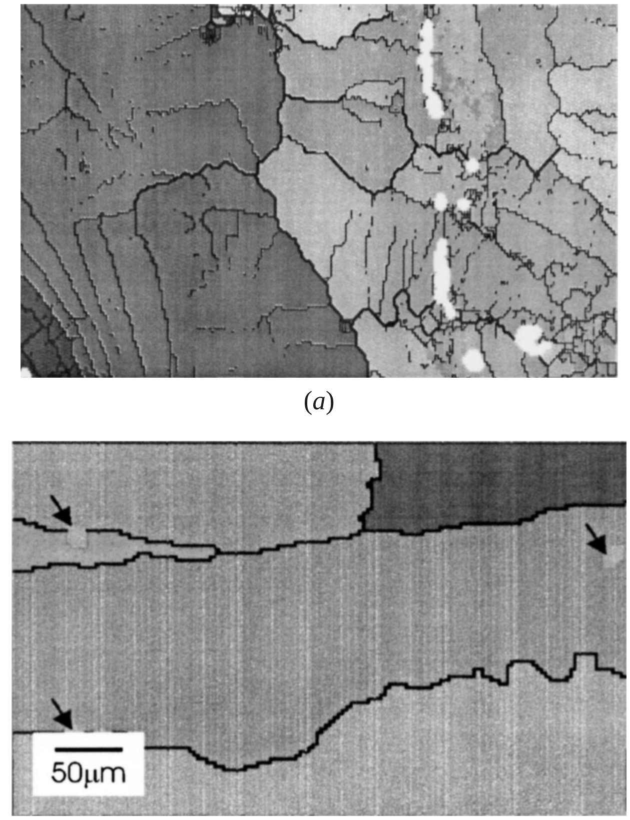

(*a*)

(*b*)

Fig. 3—Representative EBSD orientation micrographs of samples solidified in contact with a smooth substrate showing (*a*) and the as-solidified strip surface and (*b*) the ND-TD section. A given gray level represents a single austenite grain; thick lines indicate high-angle grain boundaries, while thin lines indicate low-angle boundaries (<2 deg).

B. *Microstructural Development*

Figure 3 shows EBSD orientation micrographs (derived from EBSD area scans) of both solidified surface and the through-thickness (ND-TD) section of the as-cast strip, solidified in contact with a *smooth* substrate. The nucleation density at the strip surface is low (Figure 3(a)), and coarse columnar grains grow inward in a direction essentially parallel to ND (Figure 3(b)). Figure 4 gives a similar set of EBSD micrographs for the 20 × 180 μm *ridged* substrate. Lines indicating the position of the ridges are shown in Figure 4(a) and show that the peaks of the substrate ridges may act as preferential sites for nucleation. Nevertheless, some nucleation was also possible away from the peaks of the ridges, as indicated by the isolated grains labeled in Figure 4(a). Following nucleation, selective growth and broadening of grains occurs with increasing distance from the chill surface (Figure 4(b)). The average grain width along ND-TD as a function of perpendicular distance from the chill surface is given in Figure 5(a), which shows an example of the notable effect of a ridged substrate on the development of the columnar microstructure. Figure 5(b) shows that, for a given substrate, an increase in the melt superheat also increases the grain width (i.e., decreases nucleation density) at the chill surface.

Despite the influence of the aforementioned casting variables on nucleation density in the as-cast strip, they had no significant influence on the general microstructure with all

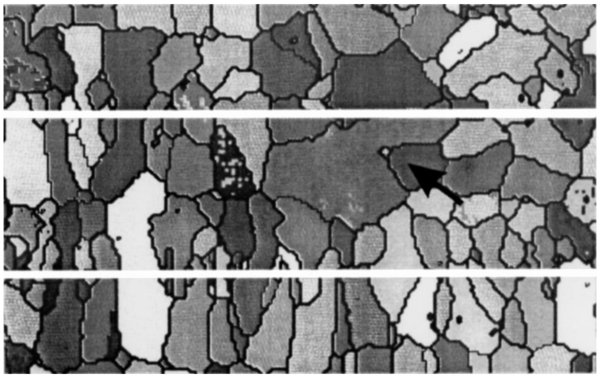

(*a*)

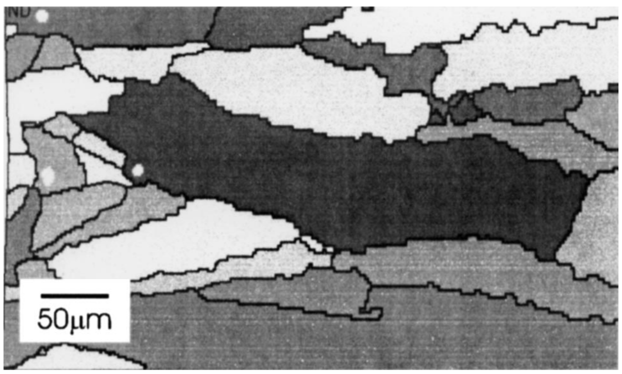

(*b*)

Fig. 4—Representative EBSD orientation micrographs of samples solidified in contact with a typical ridged substrate showing (*a*) the as-solidified strip surface where white lines indicate the position of the peaks of ridges during casting and (*b*) the ND-TD section. A given gray level represents a single austenite grain; thick lines indicate high-angle grain boundaries, while thin lines indicate low-angle boundaries (<2 deg).

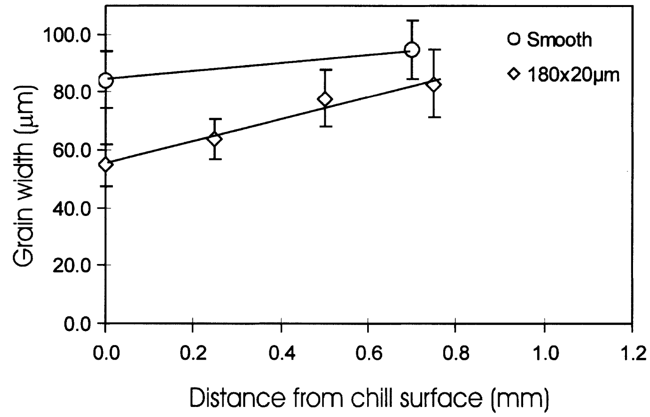

(*a*)

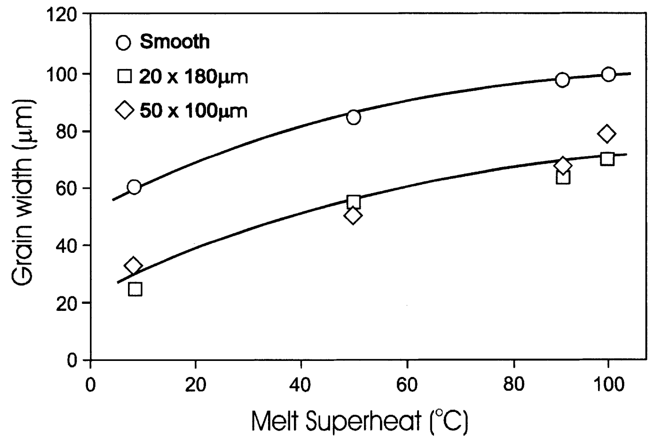

(*b*)

Fig. 5—(*a*) Average grain width ($\overline{w}$) along ND-TD as a function of perpendicular distance from the chill surface (50 °C melt superheat). (*b*) Average grain width at the chill surface ($\overline{w}_c$) as a function of melt superheat.

samples exhibiting a dispersion of second phase, which was confirmed, using EBSD, to be ferrite (Figure 6). Two types of ferrite were observed in the microstructure: cellular ferrite (γ_c) throughout the thickness of the strip with skeletal ferrite (γ_s) at 200 to 500 μm below the chill surface. The optical micrograph given in Figure 6(a) shows a region of microstructure containing both γ_c and γ_s (hardness indentations mark the boundary between these phases). Figure 6(b) is an EBSD orientation map of the area shown in Figure 6(a), which shows that both types of ferrite exist within a single austenite grain: an observation consistent for all samples.[14] During dip casting, cooling rates in excess of 10^5 °C/s are experienced at the chill surface, which are favorable conditions for nucleation and subsequent growth of austenite.[7,8,9] Subsequent rejection of Cr into interdendritic regions during solidification leads to the formation of γ_c. As the rate of solidification decreases, the primary solidifying phase changes to delta-ferrite (δ), which then partially transforms to austenite, leaving γ_s. This proposed solidification sequence generates both types of ferrite and is consistent with the observations of Mizukami and co-workers on a similar steel.[9]

C. *Solidification Textures*

Figure 7 gives {200} pole figures showing the distribution in orientation of grains at the chill surface and at a distance of 0.8 mm below the surface following solidification from a smooth and a typical ridged (20 × 180 μm) substrate. Regardless of substrate topography, grains appear almost randomly oriented at the chill surface (Figures 7(a) and (b)). During solidification, a ridged substrate generates more preferential growth of grains with their ⟨001⟩ direction almost parallel to the ND, which results in a more significant sharpening of the ⟨001⟩//ND fiber texture (Figure 7(d)) compared with the smooth substrate (Figure 7(c)).

The misorientation distribution of grains at both the chill surface and at 0.8 mm below the surface are given in Figure 8 for both a smooth and ridged (20 × 180 μm) substrate. For the ridged substrate, a near random distribution of misorientation is produced at the chill surface (Figure 8(a)), as indicated by the superimposed theoretical distribution for randomly oriented grains,[15] but this distribution changes considerably through the strip thickness (Figure 8(c)). In contrast, the smooth substrate does not generate a random distribution of misorientations at the chill surface (Figure 8(b)) and this changes only slightly through the strip thickness (Figure 8(d)).

To quantify the through-thickness gradient in texture, the mean angular deviation ($\overline{\alpha}$) of ⟨001⟩-oriented grains about ND was determined from EBSD data at various distances below the strip surface (Eq. [1]). The change in $\overline{\alpha}$ as a function of perpendicular distance from the chill surface is shown in Figure 9 for samples produced from both a smooth

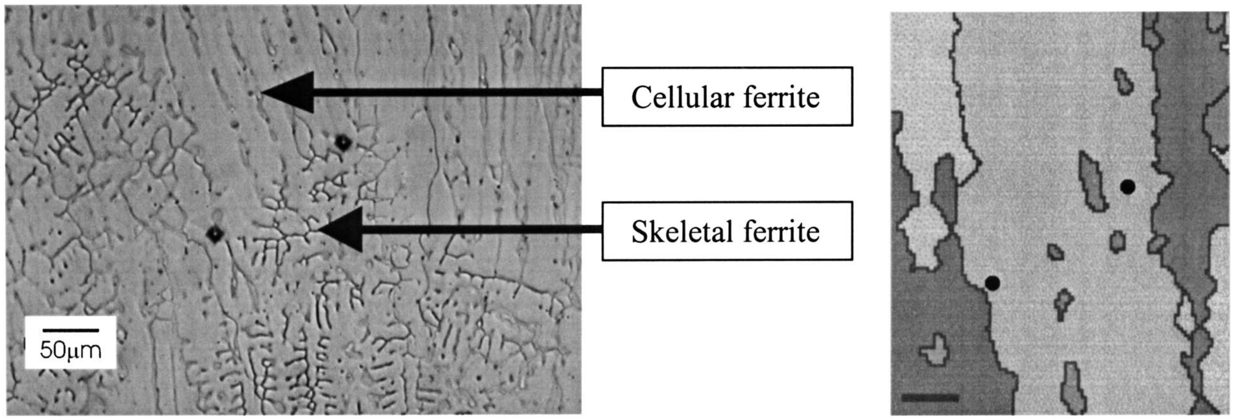

(*a*) (*b*)

Fig. 6—ND-TD section of a sample cast onto a smooth substrate: (*a*) optical micrograph showing the distinct transition in ferrite morphology; (*b*) EBSD orientation micrograph of the same area as (a), whereby a given gray level represents a single austenite grain in which the spread in Euler angles is less than 1.5 deg.

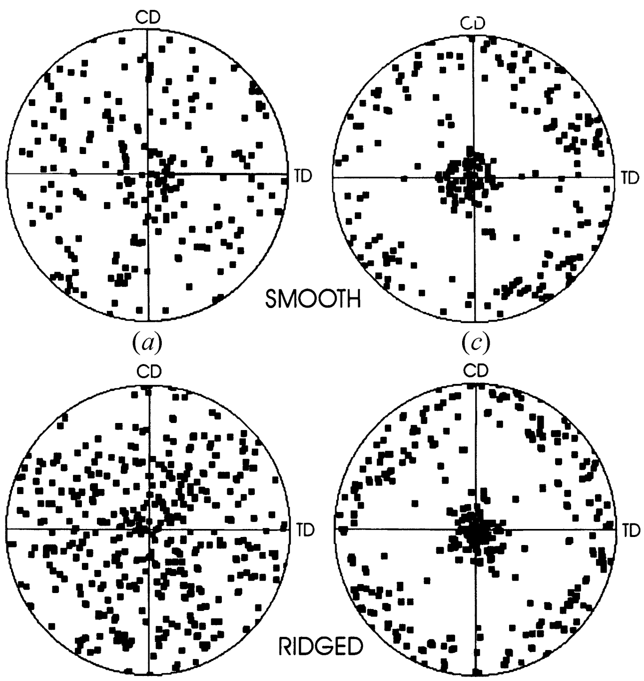

Fig. 7—{200} pole figures of discrete EBSD measurements showing the orientation spread of grains at (*a*) and (*b*) the chill surface and (*c*) and (*d*) 0.8 mm below the surface for samples produced from both a smooth and 20 × 180 μm ridged substrate (50 °C melt superheat).

and 20 × 180 μm ridged substrate. The smooth substrate results in solidification to produce $\overline{\alpha}$ of 27 deg at the strip surface, which decreases to 17 deg at a distance of 1.2 mm below the surface. Conversely, the ridged substrates produce $\overline{\alpha}$ ranging from 32 deg at the chill surface to 17 deg at a distance of 0.8 mm.

Figure 10 gives $\overline{\alpha}$, both at the chill surface and at three-quarter thickness of the strip (distance below the chill surface), as a function of average chill-surface grain width ($\overline{w}_c$) for all samples. Despite some scatter in the data, $\overline{\alpha}_c$ does not appear to be dependent on the nucleation density at the chill surface, whereas $\overline{\alpha}_{3/4}$ decreases with decreasing grain width (increasing nucleation density). For the smooth substrate, however, the data are more scattered.

IV. DISCUSSION

A. *General Solidification Behavior*

During the early stages of solidification of AISI 304 strip, both substrate topography and melt superheat were found to affect heat transfer,[10,11] which is similar to a recent study on solidification of a copper alloy by Bouchard *et al.*[16] Strezov[10] showed that substrate topography strongly affects both the degree and direction of heat flux in the melt. For a smooth substrate, heat flow was essentially perpendicular to the substrate surface (that is, opposite in direction to the solidification front). For a ridged substrate, however, the direction of heat flow was less uniform and affected by ridge dimensions, with the maximum heat flux also concentrated through the ridge peaks with a magnitude of ~5 to 10 MW/m^2 greater than that for a smooth substrate.[11] Such a difference in heat-transfer conditions appears to be sufficient to alter both the morphology of the columnar microstructure (Figures 3 through 5) and through-thickness gradient in texture (Figure 9) of the as-cast strip. Strezov and Herbertson[11] showed that an increase in melt superheat (for other casting conditions held constant) resulted in a linear decrease in the maximum heat flux and a concomitant linear decrease in nucleation density at the chill surface.

The results given in Figure 5(b) show that melt superheat is an important variable affecting the chill surface grain size, whereas depth and pitch of the ridged substrates have a smaller influence. For a given melt/substrate contact condition, an increase in melt superheat resulted in a decrease in nucleation density (Figure 5(b)). This is a common feature during casting of various metals[17] and is generally associated with an increased propensity for remelting of chill crystals formed at the mold wall, because melt superheat is increased with fewer new crystals forming on reaching the nucleation temperature as a result of a slower rate of cooling due to substrate heating. For a given melt superheat, the nucleation density was greater for a ridged substrate (Figure 5(b)), which is probably due to additional nucleation sites

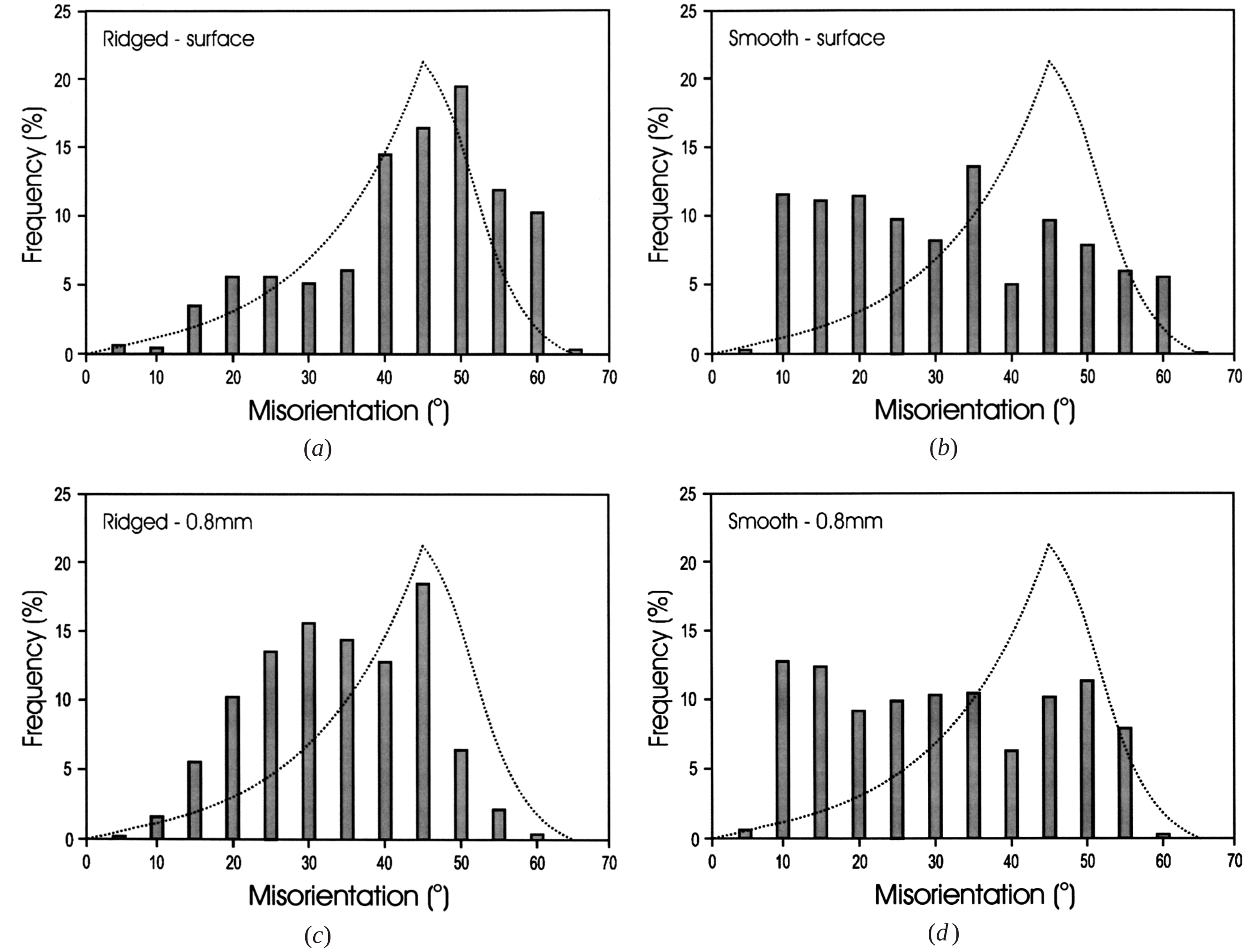

Fig. 8—Misorientation distribution of grains at (*a*) and (*b*) the chill surface and (*c*) and (*d*) 0.8 mm below the surface for samples produced from both a smooth and 20 × 180 μm ridged substrate (50 °C melt superheat).

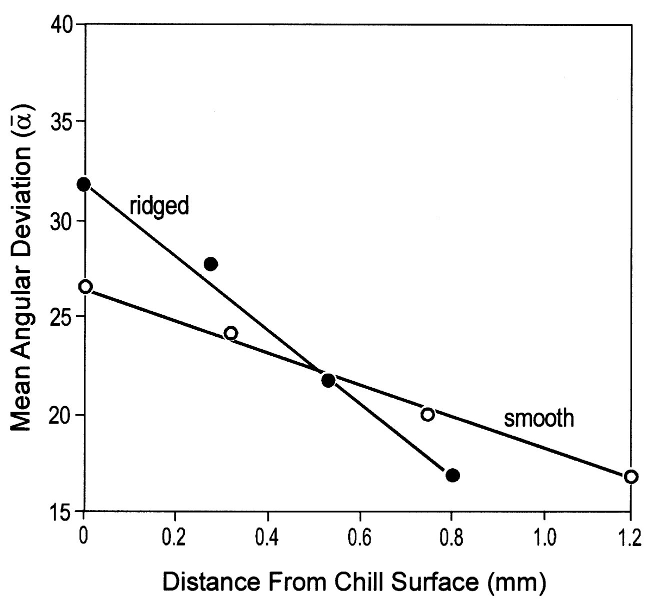

Fig. 9—Mean angular deviation ($\overline{\alpha}$) of ⟨001⟩-oriented grains about the ND as a function of distance below the chill surface for samples produced with varying substrate topography (50 °C melt superheat).

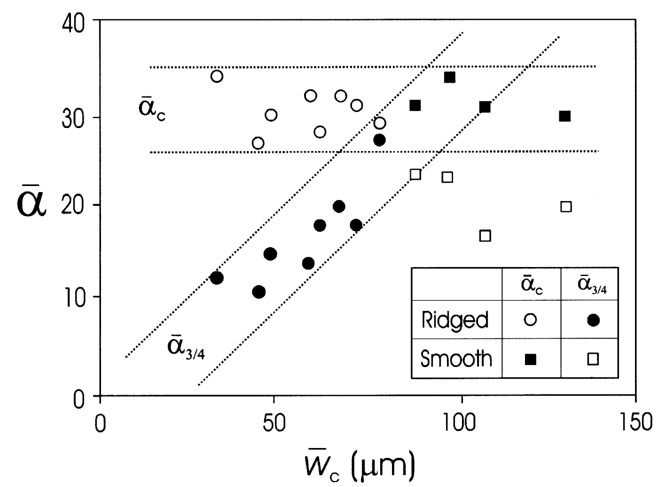

Fig. 10—Mean angular deviation ($\overline{\alpha}$) of ⟨001⟩-oriented grains about the ND both at the chill surface and three-quarter distance from the chill surface as a function of average chill-surface grain width ($\overline{w}_c$).

at the tips of the ridges together with an increase in heat flux at the initial stages of solidification (Figure 2), which equates to a higher initial rate of cooling.

B. *Control of Texture during Casting*

During conventional casting of metals, solidification usually commences by heterogeneous nucleation at the interface between the mold wall and liquid metal and results in the formation of grains with a wide range of crystallographic orientations; that is, a random texture develops.[18] Further solidification occurs by dendritic growth, whereby grains with a certain crystallographic direction aligned in the direction of heat flow (usually perpendicular to the mold wall) grow preferentially to produce the characteristic columnar zone in castings. For metals of cubic crystal symmetry, the preferred growth direction is ⟨001⟩,[17] which results in the gradual strengthening of the ⟨001⟩//ND fiber texture. The physical interpretation of this phenomenon is given in detail by other workers.[17–20] In summary, directional solidification (DS) occurs by the movement of the liquidus isotherm at a given velocity, ν_L, perpendicular to the heat flow direction. To maintain stationary growth conditions, grains oriented at an angle ϕ to the heat flow direction must grow at a higher rate than more perfectly aligned dendrites, i.e., $\nu_\theta = \nu_L/\cos\phi$.[19] Since the undercooling at a dendrite tip is a function of its growth rate,[14] for a given temperature gradient in the melt, a dendrite belonging to a misaligned grain will grow at a larger undercooling toward (or away from Ref. 19) the more favorably oriented neighboring grain. Thus, misaligned grains will have a higher local undercooling and their dendrite tips will lie slightly behind those that are better aligned with the heat-flow direction. These misaligned grains will eventually be eliminated as solidification proceeds,[17–20] with a concomitant strengthening of the ⟨001⟩ fiber texture.

The development of the ⟨001⟩ fiber texture in the as-cast strip was similar to that observed in other DS processes. The present work has shown that both substrate topography and melt superheat affect the size and shape of the columnar grains as well as the strength and through-thickness gradient in texture. Recent work by Rappaz and co-workers,[19,20] using a combination of EBSD and three-dimensional cellular automata/finite element (CAFE) modeling, have also shown that various DS processes are indeed governed by the nucleation of an essentially random distribution of grains at the substrate/melt interface, with the gradual development of the ⟨001⟩ fiber texture by growth selection.

As noted previously, nuclei with ⟨001⟩ aligned in the heat flow direction will grow most favorably, thereby impeding the growth of less favorably oriented grains. For widely spaced nuclei, all grains are expected to grow for a longer distance before impingement with neighboring grains. In addition, grains with ⟨001⟩ aligned close to the heat flow direction will also survive over a greater distance. Using a simple geometrical argument (Figure 11) and neglecting the impinging effects of secondary dendrite arms, the distance (x) that a primary dendrite arm reaches before impingement with an adjacent ⟨001⟩//ND growing dendrite is related to the distance between nuclei at the chill surface (w_c) and the angle between the growing dendrite and ND (α_c):

$$x = w_c \tan(90 - \alpha_c) \quad [2]$$

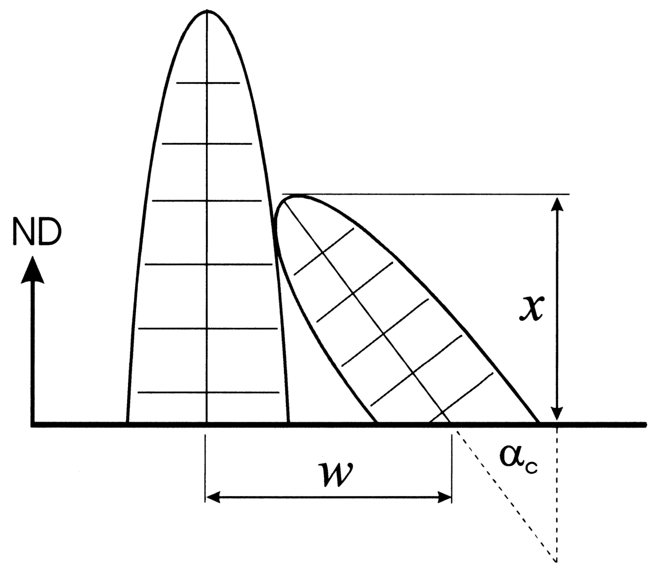

Fig. 11—Schematic diagram of two grains nucleating on a copper substrate at a given distance apart (w_c) and the distance (x) that the grain aligned at α_c to the ND can grow until impingement.

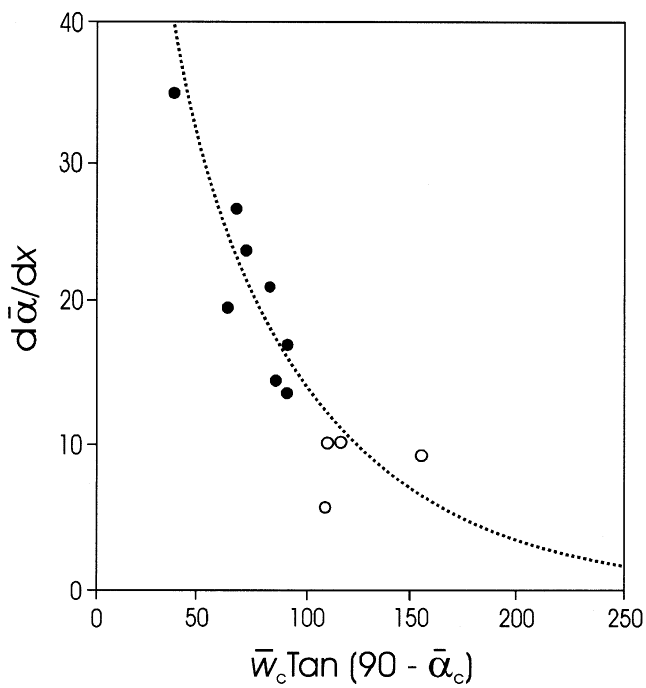

Fig. 12—$d\overline{\alpha}/dx$ as a function of casting parameters ($\overline{w}_c \cdot \tan(90 - \overline{\alpha}_c)$) for a range of samples produced at various superheats (Table I) from ridged substrates (filled symbols) and a smooth substrate (open symbols).

If it is assumed that grains nucleate with an average spacing, $\overline{w}_c$, and a mean distribution of orientations, $\overline{\alpha}_c$, Eq. [2] can be modified to estimate the change in $\overline{\alpha}$ with perpendicular distance x from the chill surface ($d\overline{\alpha}/dx \sim (\overline{\alpha}_x - \overline{\alpha}_c)/\Delta x$) as a function of both nucleation density and chill surface grain orientations:

$$d\overline{\alpha}/dx \propto \overline{w}_c \cdot \tan(90 - \overline{\alpha}_c) \quad [3]$$

A plot of $d\overline{\alpha}/dx$ as a function of $\overline{w}_c \cdot \tan(90 - \overline{\alpha}_c)$ is given in Figure 12 for all substrate types given in Table I, which shows a reasonable relationship between through-thickness texture gradient and nuclei spacing and orientation. It can be seen that $d\overline{\alpha}/dx$ tapers off at large values of $\overline{w}_c \cdot \tan (90 - \overline{\alpha}_c)$ (smooth substrate), which is probably a result of a combination of a very low nucleation density, less-than-random distribution of orientations at the chill surface, and the finite thickness of the solidified strip. With either an increase in $\overline{w}_c$ or a decrease in $\overline{\alpha}_c$, competition for growth will diminish, which is expected to decrease the rate of texture sharpening. It is relevant to note that values of $d\overline{\alpha}/dx$ in Figure 12 were calculated using an essentially constant $\overline{\alpha}_c$ value (27 to 35 deg) which indicates, for the present work, that $d\overline{\alpha}/dx$ is a simple function $\overline{w}_c$. Nevertheless, $\overline{\alpha}_c$ is not always constant and should therefore be taken into account. An extreme example was observed in a Ti-inoculated AISI 403 stainless steel,[21] where it was found that, while $\overline{w}_c$ was 46 μm, $\overline{\alpha}_c$ was less than 5 deg, which gives $\overline{w}_c \cdot \tan (90 - \overline{\alpha}_c) > 550$ and $d\overline{\alpha}/dx \sim 0$. In this special case, a uniform-width, columnar microstructure exhibiting an exceedingly sharp and constant ⟨001⟩//ND through-thickness fiber texture was produced.

The results of this study have shown that both microstructure and texture in as-cast γ-SS strip can be controlled by the manipulation of the distribution and orientation of nuclei through the choice of casting parameters: superheat and substrate topography. These parameters are known to influence the local heat-transfer conditions at the meniscus during casting.[11,22] Other factors such as immersion (casting) velocity and melt atmosphere may also control the microstructure and texture because these variables also modify the heat flux conditions at the meniscus. For example, Strezov and Herbertson[11] argued that an increase in immersion velocity enhances surface nucleation as a result of improved melt/substrate wettability. This variable can have an additional effect on the growth behavior of dendrites because it has been found that dendrites growing in a flowing melt tend to bend toward the upstream direction, with the degree of deviation affected by factors such as melt composition and flow rate.[23] Examination of the EBSD micrographs in Figures 3 and 4 indicates that, for the present steel, dendrite bending was not pronounced at a casting speed of 0.5 m/s. However, dendrite bending is expected to be more significant at higher casting speeds.[24]

V. CONCLUSIONS

A strip casting simulator was used to produce as-cast AISI 304 austenitic stainless steel strip with a microstructure similar to that produced by DSC. It was found that during casting, grains nucleate at the strip (chill) surface and nuclei with ⟨001⟩ oriented close to the heat flow direction (ND) grow favorably to produce a columnar microstructure with a slight sharpening of the ⟨001⟩//ND fiber texture. Both melt superheat and substrate topography were found to control both the nucleation density at the strip surface, which affected the coarseness of the columnar microstructure, and the through-thickness gradient in strength of the ⟨001⟩//ND fiber texture. The gradient in texture strength was related to the mean separation of nuclei and the average angle between ⟨001⟩ and the solidification direction. By controlling these casting parameters, it is possible to produce strip-cast austenitic stainless steel exhibiting a given microstructure and texture and, hence, control the mechanical and physical properties of the as-cast strip.

ACKNOWLEDGMENTS

The authors express their gratitude to Drs. L. Strezov and K. Mukunthan (BHP Billiton) for kindly supplying the as-cast coupons and heat-transfer data, and for many useful discussions. One of the authors (AH) is grateful to the Australian Research Council for a postgraduate scholarship.

REFERENCES

1. M.M. Wolf: *Proc. Int. Conf. on Near-Net-Shape Casting in the Minimills*, Vancouver, Canada, J.K. Brimacombe and I.V. Samarasekera, eds., Canadian Institute of Mining, Metallurgy and Petroleum, 1995, p. 3.
2. P.A. Manohar, M. Ferry, and A. Hunter: *Mater. Forum*, 2000, vol. 24, p. 19.
3. A.W. Cramb: *Proc. Int. Conf. on Near-Net-Shape Casting in the Minimills*, Vancouver, Canada, J.K. Brimacombe and I.V. Samarasekera, eds., Canadian Institute of Mining, Metallurgy and Petroleum, 1995, p. 355.
4. W. Blejde, R. Mahapatra, and H. Fukase: *Proc. Belton Memorial Symp.*, Sydney, ISS, 2000, p. 253.
5. K. Mukunthan, L. Strezov, R. Mahapatra, and W. Blejde: *Proc. J.K. Brimacombe Memorial Symp.*, Vancouver, Canada, I.V. Samarasekera, ed., 2000, p. 102.
6. J.A. Brooks and A.W. Thompson: *Int. Mater. Rev.*, 1991, vol. 36, p. 16.
7. T. Koseki and M.C. Flemings: *Metall. Mater. Trans. A*, 1995, vol. 26, p. 2991.
8. T. Koseki and M.C. Flemings: *Metall. Mater. Trans. A*, 1997, vol. 26, p. 2385.
9. H. Mizukami, T. Suzuki, and T. Umeda: *Mater. Sci. Eng. A*, 1993, vol. 17, p. 363.
10. L. Strezov: Ph.D. Thesis, University of Newcastle, Newcastle, Australia, 1994.
11. L. Strezov and J. Herbertson: *Iron Steel Inst. Jpn. Int.*, 1998, vol. 38, p. 959.
12. J. Beck, B. Blackwell, and C.R. St. Clair: *Inverse Heat Conduction—Ill-Posed Problems*, John Wiley & Sons, New York, NY, 1985.
13. A. Hunter: Ph.D. Thesis, University of Wollongong, Wollongong, Australia, 2002.
14. A. Hunter and M. Ferry: *Scripta Mater.*, 2002, vol. 46, p. 253.
15. J.K. Mackenzie: *Biometrica*, 1958, vol. 45, p. 229.
16. D. Bouchard, F.G. Hamel, I.-P. Nadeau, S. Bellemare, F. Dreneau, D.-A. Tremblay, and D. Simard: *Metall. Mater. Trans. B*, 2001, vol. 32B, p. 111.
17. B. Chalmers: *Principles of Solidification*, John Wiley & Sons, New York, NY, 1967.
18. D. Walton and B. Chalmers: *Trans. AIME*, 1959, vol. 215, p. 447.
19. C.-A. Gandin and M. Rappaz: *Acta Metall. Mater.*, 1994, vol. 42, p. 2233.
20. C.-A. Gandin, M. Rappaz, D. West, and B.L. Adams: *Metall. Mater. Trans A*, 1995, vol. 26A, p. 1543.
21. A. Hunter and M. Ferry: *Metall. Mater. Trans. A*, 2002, vol. 33A, p. 1499.
22. R.I.L. Guthrie, M. Isac, J.S. Kim, and R.P. Tavares: *Metall. Mater. Trans. B*, 2000, vol. 31B, p. 1031.
23. H. Esaka, F. Suter, and S. Ogibayashi: *Iron Steel Inst. Jpn. Int.*, 1996, vol. 36, p. 1264.
24. H. Takani, C.-A. Gandin, and M. Rappaz: *Acta Mater.*, 2000, vol. 48, p. 675.